Biosensors and Bioelectronics 208 (2022) 114234

Contents lists available at ScienceDirect

Biosensors and Bioelectronics

journal homepage: www.elsevier.com/locate/bios

Microneedle patches integrated with lateral flow cassettes for blood-free chronic kidney disease point-of-care testing during a pandemic

Yi-Jyun Chen [a,1], Ying-Pei Hsu [a,b,1], You-Lin Tain [c,d,1], Nan-Si Li [a], Hao-Han Pang [a], Shiao-Wei Kuo [b,e,*], Hung-Wei Yang [a,**]

[a] Institute of Medical Science and Technology, National Sun Yat-Sen University, Kaohsiung 80424, Taiwan
[b] Department of Materials and Optoelectronic Science, Center for Functional Polymers and Supramolecular Materials, National Sun Yat-sen University, Kaohsiung 80424, Taiwan
[c] Department of Pediatrics, Kaohsiung Chang Gung Memorial Hospital and Chang Gung University College of Medicine, Kaohsiung 83301, Taiwan
[d] Institute for Translational Research in Biomedicine, Kaohsiung Chang Gung Memorial Hospital and Chang Gung University College of Medicine, Kaohsiung 83301, Taiwan
[e] Department of Medicinal and Applied Chemistry, Kaohsiung Medical University, Kaohsiung 80708, Taiwan

ARTICLE INFO

Keywords:
Cystatin C
Chronic kidney disease
Interstitial fluid
Lateral flow immunosensor
Microneedles

ABSTRACT

Chronic kidney disease (CKD) is the most neglected chronic disease affecting over 750 million persons in the world. Currently, many patients with cancers or other chronic diseases (i.e., CKD) struggle to receive clinical treatment or examination due to hospitals cancelling or delaying in the COVID-19 pandemic, which may increase the risk of death. Cystatin C (Cys C) has been proposed as a potential glomerular filtration rate (GFR) marker for the early detection of acute kidney injury and CKD. However, most traditional methods for Cys C detection are immunoassays using serum as a sample and are tedious to perform and economically burdensome. To diagnose the disease in the early stage and carry out daily management during the current pandemic, we developed an integration of hydrogel microneedle patch (HMNP) and lateral flow cassette (LFC) to rapidly detect Cys C in skin interstitial fluid (ISF) in 25 min for blood-free CKD management anytime and anywhere by the naked eye that can reduce the impact of an individual's quality of life and life expectancy. Conceivably, this strategy presents a wide scope in the application of numerous other diseases if corresponding analytes are available in skin ISF.

1. Introduction

Chronic kidney disease (CKD) is defined as kidney damage for at least three months or over three months. To date, CKD is the fourth most common noncommunicable form of kidney malfunction, characterized by progressive loss of function of the renal tubules. Increasing evidence has established that CKD is associated with an increased risk for cardiovascular disease mortality and is a risk multiplier in patients with hypertension and diabetes (Sarnak et al., 2003). In the United States (US), approximately 15% of US adults are estimated to have CKD-that is, approximately 37 million people. However, as many as 9 in 10 adults with CKD do not know they have CKD, and approximately 2 in 5 adults with severe CKD do not know they have CKD (Vart et al., 2020), resulting in considerable Medicare costs (over USD$81.8 billion) for people with CKD, or USD$23,700 per person. Therefore, finding this disease early and treating it early is the best solution to solve the above dilemma. Currently, estimation of the glomerular filtration rate (eGFR) value is one of the prominent criteria for the diagnosis of CKD (<60 mL/min/1.73 m^2) in hospitals. The normal value in young adult men and women is approximately 125 mL/min/1.73 m^2. Values below 15 mL/min/1.73 m^2 indicate kidney failure, and the person can be identified as a candidate for dialysis or renal replacement therapy/kidney transplantation (Biljak et al., 2017). However, eGFR-based CKD diagnosis is tedious and currently possible for stage III-V CKD patients. Inability to curb the progression of CKD leads to acute kidney failure (stage V) and mortality (Neild, 2017). Hence, the necessity arises to

* Corresponding author. Department of Materials and Optoelectronic Science, Center for Functional Polymers and Supramolecular Materials, National Sun Yat-sen University, Kaohsiung 80424, Taiwan.
** Corresponding author. Institute of Medical Science and Technology, National Sun Yat-sen University, Kaohsiung 80424, Taiwan.
E-mail addresses: kuosw@faculty.nsysu.edu.tw (S.-W. Kuo), howardyang@mail.nsysu.edu.tw (H.-W. Yang).
[1] Y.J. Chen, Y.P. Hsu, and Y.L. Tain contributed equally to this work.

https://doi.org/10.1016/j.bios.2022.114234
Received 16 December 2021; Received in revised form 27 March 2022; Accepted 28 March 2022
Available online 31 March 2022

develop facile and non-invasive diagnostics to detect CKD patients at stages I and II, even earlier. In addition, a previous report highlighted that patients with severe forms of CKD have a very high risk of COVID-19 mortality, which is even higher than that of other known high-risk groups, including patients with hypertension, obesity, chronic heart disease or lung disease (Gansevoort and Hilbrands, 2020). Therefore, a non-invasive sampling and real-time testing for CKD monitoring without going to the hospital is an urgent need through the midst of pandemic.

To date, several biomarkers have been reported for CKD, such as creatinine (Cr), neutrophil gelatinase-associated lipocalin (NGAL), kidney injury molecule-1 (KIM-1), liver-type fatty acid binding protein (L-FABP) and cystatin C (Cys C). Among them, Cys C has been identified as an early biomarker of renal disease with confirmed prognostic implications progression because it tends to be reabsorbed by healthy kidneys (Uchida and Gotoh, 2002; Sharma et al., 2011). In addition, Cys C is not associated with variation in age, sex and dietary intake of individuals compared with other biomarkers of CKD (Grubb et al., 2005). Therefore, many types of biosensing technologies have been developed to measure Cys C levels for CKD monitoring, such as fluorescence resonance energy transfer (FRET)-based biosensors (Wang et al., 2021), surface plasmon resonance-based biosensors (Lesnak et al., 2021), and electrochemistry-based biosensors (Desai et al., 2018; Lopes et al., 2019; Devi and Krishnan, 2020), but the methods are time-consuming, expensive, tedious and require trained manpower and sophisticated equipment, which may not be present universally. In addition, most of these approaches require withdrawing fresh blood, which is painful and inconvenient with potential risk for cross-contamination, especially when the lancet is reused or not properly sterilized. Additionally, the test result is typically not available until three days later. Although the sweat from the eccrine sweat gland can be easily obtained and the sweat-based biosensors can be used for real-time monitoring of personal health states, the concentration of biomarkers with high molecular weights in sweat is significantly lower than that in other body fluid samples (i.e., serum and interstitial fluid (ISF)) with a similar volume. The main reason behind this huge difference is the filtration of extracellular matrix tight junctions, which limits the size of biomolecules that can pass through the skin (Xu et al., 2021). Thus, the ISF from the skin is a viable minimally invasive fluid that has considerable advantages in the diagnosis and real-time physiological monitoring (Samant et al., 2020). However, conventional methods for ISF extraction, such as a suction blister, depth-limited hypodermic cannula, and open-flow microperfusion, are time-consuming and risky to patients and require medical expertise and specialized instruments (Nilsson et al., 2019; Bodenlenz et al., 2016). To address the above issues, microneedles (MNs) fabricated from metal or hydrogel have been proposed to extract skin ISF using a painless and minimally invasive strategy (Madden et al., 2020; Zheng et al., 2020). Moreover, manufactured MNs should have the ability to obtain a sufficient volume of ISF with rapid extraction speed to increase sample integrity and patient compliance and expand the range of applicable biomarkers (Kim et al., 2021).

Therefore, there is an urgent need for more reliable biosensing devices to provide timely feedback to patients diagnosed with CKD. In this study, we demonstrated on-site, blood-free, and easy CKD monitoring during a pandemic (i.e., COVID-19) by integrating MN extraction with a lateral flow cassette (LFC). To collect a larger volume of skin ISF in a shorter period, we added absorbent material, sodium polyacrylate (PAA-Na), into poly(methyl vinyl ether-alt-maleic acid) (PMVE/MA)-based hydrogel MNs (HMNs) to increase the swelling and water holding capabilities. We further designed an LFC containing a lateral flow paper strip and a square sample port for hydrogel microneedle patch (HMNP) assembly to run a Cys C immunoassay using MN-extracted ISF samples (Scheme 1A). Using this integration of HMNP and LFC, we demonstrated that CKD patients can complete Cys C testing by themselves within 25 min to achieve CKD management anytime.

2. Experimental methods

2.1. Materials

Poly(methyl vinyl ether-alt-maleic acid) (PMVE/MA, Mw ~1,980,000 by LS, average Mn ~960,000), polyethylene glycol 8000 (PEG_{8000}), sodium carbonate (Na_2CO_3), hydrogen tetrachloroaurate trihydrate ($HAuCl_4$), sodium citrate ($Na_3C_6H_5O_7$), horseradish peroxidase (HRP, 198 units/mg solid), bovine serum albumin (BSA), BSA-fluorescein isothiocyanate conjugate (BSA-FITC), and sodium polyacrylate (PAA-Na) were purchased from Sigma–Aldrich (St. Louis, MO, USA). Traut's reagent, goat anti-rabbit IgG antibody, Cys C recombinant

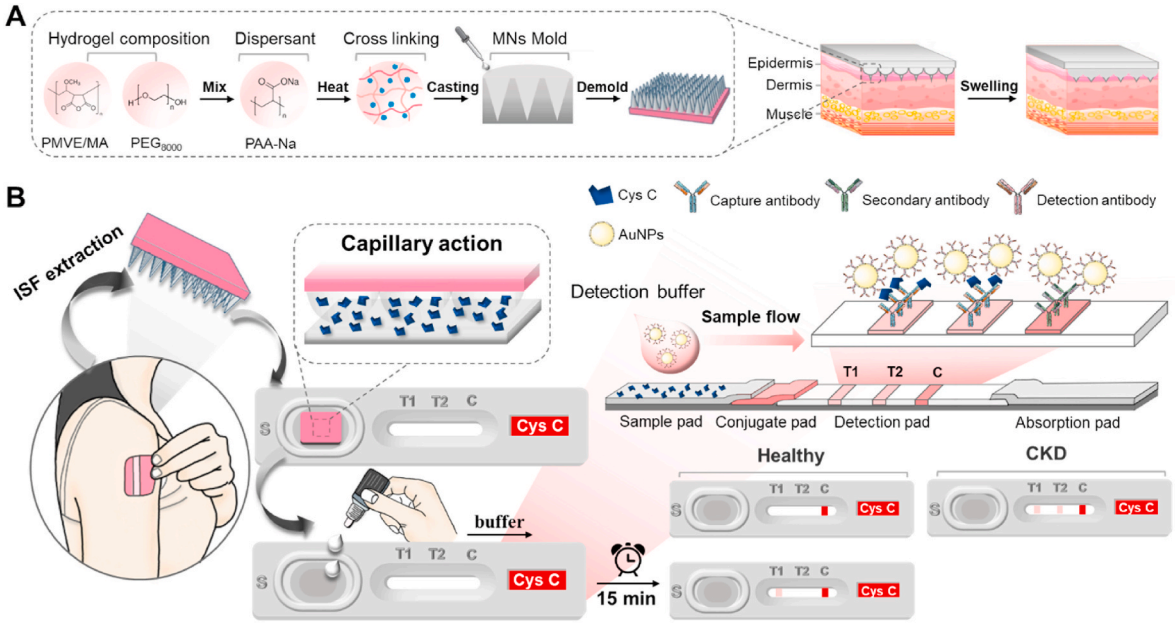

Scheme 1. (A) The preparation procedure of HMNPs. (B) Schematic of the proposed blood-free rapid detection for Cys C and the detection mode for the healthy and CKD subjects.

human protein, and polyacrylamide desalting column were purchased from Thermo Scientific (Waltham, Massachusetts, USA). Rabbit anti-Cys C monoclonal antibody ($Ab_{Cys\ C}$), rabbit anti-PSA monoclonal antibody (Ab_{PSA}), and rabbit anti-EGFR monoclonal antibody (Ab_{EGFR}) were purchased from Proteintech (Rosemont, IL, USA). Lateral flow paper strips were purchased from Advance Bio-Pharmaceutical, Taiwan.

2.2. Fabrication and modification of gold nanoparticles (AuNPs)

First, AuNPs were prepared by sodium citrate reduction of $HAuCl_4$ according to our previous report with minor modifications (Hsu et al., 2020a). Briefly, a sodium citrate solution (100 mL, 38.8 mM) was boiled at 100 °C in a microwave oven, after which 1 mL of $HAuCl_4$ (1 M) solution was quickly added to the boiling solution, and the mixture was allowed to react above 100 °C for 15 min with a condenser to prevent solvent evaporation. After the solution colour changed from pale yellow to wine red, the solution was gradually cooled to room temperature. Finally, the wine red colour solution was cooled and washed two times with DI-H_2O, followed by storage in gold buffer at 4 °C for further use.

For modification of AuNPs with antibodies, 90 μL (100 μg/mL) of thiolated $Ab_{Cys\ C}$ (SH-$Ab_{Cys\ C}$) was mixed with 400 μL ($OD_{520\ nm} = 0.5$) of prepared AuNP solution on an orbital shaker in the dark for 1 h, followed by the addition of 10 μL (20 mg/mL) of HRP for another 1 h. The mixed solution was then centrifuged (12,000 rpm, 10 min) and fully washed with tris-buffered saline with 0.1% Tween 20 detergent (TBST) to remove unreacted SH-$Ab_{Cys\ C}$ and HRP to obtain HRP-blocked AuNPs/$Ab_{Cys\ C}$ (HRP-*b*-AuNPs/$Ab_{Cys\ C}$). Furthermore, we used a rat Cys C enzyme-linked immunosorbent assay (ELISA) kit and followed the manufacturer's protocols to determine the concentration of SH-$Ab_{Cys\ C}$ immobilized on AuNPs. The absorbance spectrum and the zeta potential of prepared AuNPs were analysed with UV/Vis/NIR spectroscopy (MODEL V-700, JASCO, Japan) and dynamic light scattering (DLS, SZ-100, HORIBA, Japan). The morphology and particle size of the prepared AuNPs were characterized by transmission electron microscopy (TEM, H-7500, Hitachi).

2.3. Fabrication of hydrogel MNPs (HMNPs)

All HMNPs were fabricated by casting solutions in female PDMS moulds using scraping and pressing procedures. We first prepared a casting solution containing PMVE/MA (15 wt%), PEG_{8000} (7.5 wt%), Na_2CO_3 (3 wt%), and PAA-Na (0.2 wt%) at 60 °C for 2 h. Furthermore, 30 μL of the casting solution was cast on PDMS moulds followed by centrifugation (3,500 rpm 3 min) and vacuuming at room temperature for 0.5 h to fill the cavities, and the solution in the cavities was dried at room temperature under vacuum for 8 h to solidify into MNPs. In order to make the MNPs heat more evenly and have better crosslinking efficiency, the MNPs were first carefully removed from the PDMS moulds using bandages and then put into an oven at 80 °C for 48 h for crosslinking to obtain HMNPs (Scheme 1A). The morphology of the prepared MNs was characterized by scanning electron microscopy (SEM, SU8220, Hitachi).

2.4. Mechanical strength test

Tests of the mechanical properties of HMNPs were performed using a displacement-force test station (Model 921A, Tricor Systems Inc., Elgin, IL, USA), as described previously (Hsu et al., 2020b). The initial gauge was set as 2.00 mm between the tip of the single MN and the stainless steel plate, a single MN was attached to the mount of a moving sensor, and an axial force (10 N) was applied to move the mount at a speed of 500 μm/min. The mount pressed the single MN against a flat, rigid surface of stainless steel oriented perpendicularly to the axis of mount movement. The failure force of the single MN was recorded as the needle began to buckle.

2.5. Swelling assay of HMNPs

HMNPs were inserted in agarose gel PBS solution for 2 min to an equilibrium state. The weight of HMNP before and after insertion was used to calculate the swelling ability of HMNP based on the following equation (Pacielloab and Santonicola, 2015):

$$R_{sw} = \frac{W_{swollen}}{W_{dry}}$$

where R_{sw}, $W_{swollen}$, and W_{dry} are the swelling ratio, dry weight of HMNP, and swollen weight of HMNP, respectively.

2.6. Ex vivo ISF extraction efficiency using HMNPs

To determine whether the HMNPs could penetrate skin to extract skin ISF, the patches were inserted into full-thickness, shaved pig cadaver skin with the subcutaneous fat removed. HMNPs were inserted into the skin by pressing against the backside of an HMNP with a thumb using a force of approximately 1.5 N and then removed after 10 min of HMNP insertion. Next, the inserted area of skin was visualized, and images of the microneedle-punctured skin were collected using fluorescence stereomicroscopy (SZX7; Olympus Corp., Tokyo, Japan). To assess the skin ISF extraction capacity of HMNPs, pig cadaver skin was soaked in PBS solution containing rhodamine b (0.48 kDa), mCherry (31 kDa), and BSA-FITC (67 kDa) overnight. After drying the porcine skin surface with paper towel, HMNPs were thumb pressed into the porcine skin and kept for 2 min. The swollen HMNPs were observed by fluorescence stereomicroscopy to assess the status of ISF extraction. The weights of HMNPs before and after the application were also recorded and calculated for skin ISF extraction volume per patch (V_{ISF}) according to the following equation (Zheng et al., 2020):

$$V_{ISF} = \frac{W_{swollen} - W_{dry}}{\rho}$$

where ρ is the density of body ISF and is assumed to be 1 g/mL.

2.7. In vivo skin ISF extraction efficiency of HMNPs

All animal studies were approved by the Institutional Animal Ethics Committee (IACUC) of Chang Gung Memorial Hospital (Permit Number: 2020031602). The HMNPs were inserted into the skin by pressing against the backside of a microneedle patch with a thumb using a force of approximately 1.5 N, and then removed after 5 min of insertion. Next, the inserted area of skin was visualized by fluorescence stereomicroscopy to observe the level of skin recovery after HMNP insertion. In addition, the weights of HMNPs before and after the application were also recorded to calculate the skin ISF extraction volume per patch (V_{ISF}).

2.8. Preparation of LFC for Cys C rapid test

All materials for the LFC were obtained from Millipore (Billerica, USA). The main components of an integrated LFC, which mainly include a sample pad (CFSP001700), a conjugated pad (GFCP00080000), a glass fiber detection pad (GFDX203000), and an absorption pad (CFSP001700) assembled on a plastic backplane (HF000MC100) in sequence, are then put in a cassette with a square sample port for HMNP assembly. The sample pad and conjugated pad were pretreated with 0.01 M PBS containing 3% BSA and 0.05% Tween-20 (v/v) and then dried at 50 °C for 2 h. The control line (C line) and two test lines (T1 and T2 lines) were stamped with goat anti-rabbit IgG antibody (1 mg/mL) and $Ab_{Cys\ C}$ (0.5 or 1 or 1.5 or 2 mg/mL for T1 line and 0.5 mg/mL for T2 line) on the surface of the detection pad, respectively, and dried at 37 °C for 2 h to obtain $LFC_{Cys\ C}$.

2.9. Sensitivity, specificity, and selectivity of LFC

To determine the sensitivity, we prepared different concentrations of Cys C ranging from 0 μg/mL to 5 μg/mL and added them to HRP-*b*-AuNPs/$Ab_{Cys\ C}$ in running buffer. Subsequently, the mixed solution (20 μL) was added to the sample pad of the LFC, followed by the addition of an extra 80 μL running buffer for 15 min to observe the imprint of lines. For specificity test, the two test lines were stamped with Ab_{PSA} to obtain LFC_{PSA} or with Ab_{EGFR} to obtain LFC_{EGFR} (1 mg/mL for T1 line and 0.5 mg/mL for T2 line), followed by running the test with 5 μg/mL of Cys C according to the procedure mentioned above. In addition, the selectivity of LFC was also studied by testing several different control proteins, including interleukin-2 (IL-2), interleukin-4 (IL-4), interleukin-13 (IL-13), and interferon-γ (IFN-γ), at 3 μg/mL, which was used as a negative control, and PBS was used as a blank control.

2.10. Storage stability of $LFC_{Cys\ C}$

The accelerated ageing test of the $LFC_{Cys\ C}$ was performed according to the Arrhenius model to evaluate the storage stability of $LFC_{Cys\ C}$. The prepared $LFC_{Cys\ C}$ were stored at room temperature (25–28 °C) and 37° in the dark for different periods (1–28 days) and then used to detect 5 μg/mL Cys C protein at each time point. The stability of the stored $LFC_{Cys\ C}$ was evaluated by comparing their line intensities with their initial line intensities at Day 0. All measurements were performed in triplicate for accurate calculations to develop a standard protocol.

2.11. Cys C rapid detection in skin ISF from CKD rats

The *in vivo* efficacy of the HMNP-integrated $LFC_{Cys\ C}$ for the Cys C rapid test was evaluated in adenine (0.25 mg/kg/day)-induced adult CKD rats based on our previous studies (Chang et al., 2021). Before HMNP insertion, the rats were anaesthetized with 2% isoflurane gas for all experiments, and their back hair was removed using an electric shaver and cream hair remover. Subsequently, HMNP was pressed on the backs of normal rats or CKD rats for 5 min and then removed to the square sample port of $LFC_{Cys\ C}$ for transference of the extracted ISF to the sample pad of $LFC_{Cys\ C}$ from HMNP. One minute later, the HMNPs were removed, followed by the addition of an extra 80 μL running buffer containing HRP-*b*-AuNPs/$Ab_{Cys\ C}$ for 15 min to observe the imprint of lines. Furthermore, we also used the rat Cys C ELISA kit (Catalogue: 201281, Abcam) to determine the Cys C concentrations in rat skin ISF (extracted by suction blister) and in rat serum samples to prove the detection accuracy of our rapid testing system.

2.12. Statistics

The data are expressed as the mean ± SD based on at least three independent experiments. Statistical analysis was performed using Student's *t*-test. Differences were considered statistically significant if $^*p < 0.05$.

3. Results and discussion

3.1. Mechanism of the proposed HMNP-integrated $LFC_{Cys\ C}$

In this research, we proposed a blood-free PoC kit comprising HMNP and $LFC_{Cys\ C}$ for rapid CKD testing during the pandemic. Scheme 1B shows the principle of $LFC_{Cys\ C}$ detection of Cys C. HMNP was first pressed on the skin (i.e., human arm) for 5 min and then removed to the square sample port of $LFC_{Cys\ C}$, the extracted ISF in MNs would be transferred to the sample pad of $LFC_{Cys\ C}$ by capillary action. One minute later, the HMNPs were removed, followed by the addition of running buffer containing HRP-*b*-AuNPs/$Ab_{Cys\ C}$ for 15 min to display the imprint of lines. For people with a high risk of CKD (with abnormal Cys C concentration), more HRP-*b*-AuNPs/$Ab_{Cys\ C}$-Cys C are formed, which cannot completely be captured by the T1 line, resulting in the C, T1, and T2 lines appearing red colour. Conversely, for healthy people (with normal Cys C concentrations), fewer HRP-*b*-AuNPs/$Ab_{Cys\ C}$-Cys C are formed, which can be completely captured by the T1 line to display the only C line or C/T1 lines. Thus, the proposed HMNP-integrated $LFC_{Cys\ C}$ can be used by patients with CKD to assess whether their CKD is well controlled within 25 min at home during a pandemic (especially during the COVID-19 pandemic).

3.2. Characterization of AuNPs and modification of AuNPs

The synthesized AuNPs had good dispersity and uniformity with the characteristic colour of red wine, and a single absorption peak at 520 nm was found (Fig. 1B). The morphology and size of the prepared AuNPs were characterized by TEM and dynamic light scattering (DLS), with an average size of 21 ± 2.8 nm (Fig. 1A). After conjugation with $Ab_{Cys\ C}$, the absorption peak of AuNPs was shifted to 525 nm from 520 nm and then further shifted to 532 nm after adsorption of HRP for blocking, indicating the successful immobilization of $Ab_{Cys\ C}$ and HRP on the surface of AuNPs. The results were also confirmed by TEM; each AuNP was covered with a light grey ring with an average size of 27 ± 1.9 nm after immobilization of $Ab_{Cys\ C}$ and HRP compared with naked AuNPs (Fig. 1A).

To form AuNPs/$Ab_{Cys\ C}$, thiolated $Ab_{Cys\ C}$ was reacted with and bound to AuNPs through Au–S bonds formed between the AuNPs and thiolated antibodies. Successful $Ab_{Cys\ C}$ binding was confirmed by measuring the unbound $Ab_{Cys\ C}$ in the supernatant using ELISA, and approximately 6.9 ± 0.5 μg of $Ab_{Cys\ C}$ bound to 50 μg of AuNPs with a conjugation efficiency of 76.7 ± 5.6% was selected as a signal probe for Cys C detection (Fig. 1C). Furthermore, the successful adsorption of HRP on the surface of AuNPs/$Ab_{Cys\ C}$ to form HRP-*b*-AuNPs/$Ab_{Cys\ C}$ for blocking was confirmed by TMB assay. The results showed that TMB was oxidized by HRP-*b*-AuNPs/$Ab_{Cys\ C}$ to appear yellow in acidic solution, and a new absorption peak appeared at 450 nm compared with naked AuNPs, indicating that HRP was indeed adsorbed on the surface of AuNPs/$Ab_{Cys\ C}$ to block nonspecific adsorption (Fig. 1D). Approximately 95 ± 3.7 μg of HRP adsorbed onto 50 μg of AuNPs/$Ab_{Cys\ C}$ with a conjugation efficiency of 47.5 ± 1.9% (Fig. 1E).

3.3. Characterization of HMNPs

To examine this hypothesis, we developed HMNPs made of swelling PMVE/MA-based hydrogel, of which the swelling ratio was controlled by the added concentration of PEG_{8000} (as crosslinker) and PAA-Na (as absorbent material). HMNPs were prepared based on the crosslinking reaction between carboxylic acid groups (-COOH) of PMVE/MA and alcoholic groups (-OH) of PEG_{8000} at elevated temperature (80 °C) to form ester groups. Controlling the swelling ability means that the ISF extraction rate can be manipulated to a desired rate by altering the degree of crosslinking (Donnelly et al., 2014). Thus, how to prepare an HMNP with high mechanical strength and a super swelling ratio for excellent extraction of skin ISF is urgently needed. We first investigated the influence of the PAA-Na content in the formulation (20% w/w PMVE/MA, 15% w/w PEG_{8000}, 3% w/w Na_2CO_3) on the swelling ratio. The results demonstrated that the percentage swelling increased to 442% from 382% (0% w/w PAA-Na) after adding 0.2% w/w PAA-Na to the formulation, and the percentage swelling was also higher than 0.5% w/w PAA-Na, most likely because too much PAA-Na will reduce the crosslinking degree of HMNP to cause part of the HMNP to be dissolved (Fig. S1). In addition, no significant toxicity towards HUVECs was observed when the formulation contained PAA-Na (Fig. S2).

We then investigated the influence of the ratio between PMVE/MA and PEG_{8000} on the swelling ratio. Swelling curves were constructed for each of the HMNPs, and their percentage swelling over time is shown in Fig. 2A. We found that HMNPs containing 15% w/w PMVE/MA, 3% w/w Na_2CO_3, and 0.2% w/w PAA-Na crosslinked with 7.5% w/w PEG_{8000}

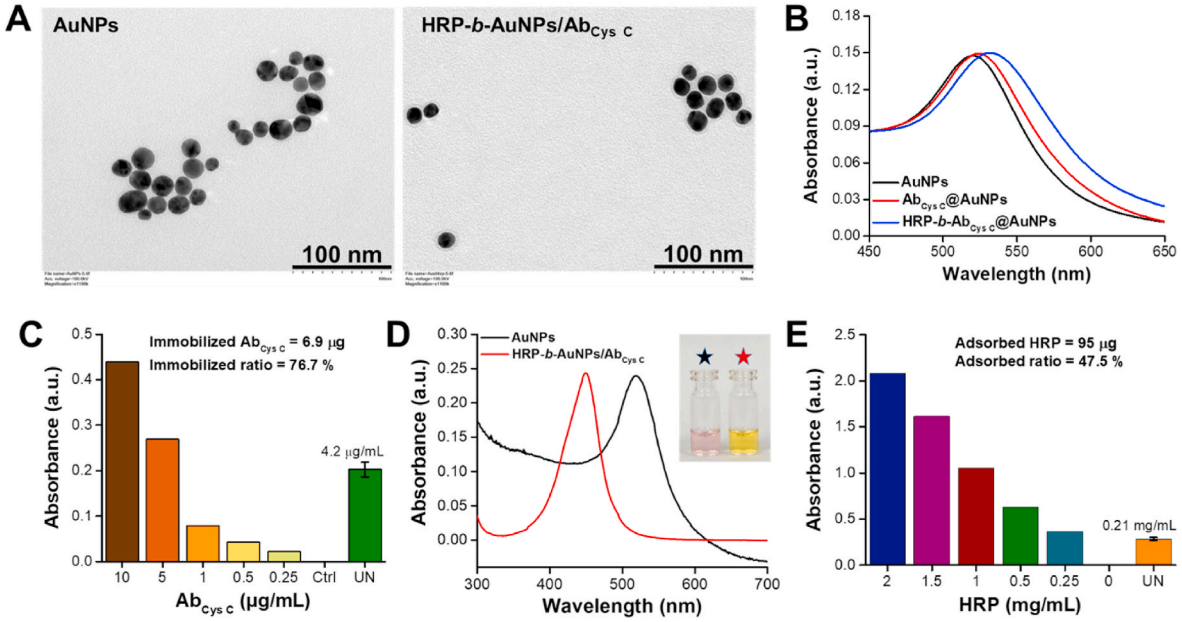

Fig. 1. (A) TEM images of prepared AuNPs and HRP-*b*-AuNPs/$Ab_{Cys\ C}$. (B) UV–vis absorption spectra of AuNPs before and after different conjugates. (C) Amount of $Ab_{Cys\ C}$ bound per 50 μg of AuNPs and the corresponding immobilized ratio (n = 3). (D) TMB assay of HRP coated on AuNPs/$Ab_{Cys\ C}$ to confirm the successful formation of HRP-*b*-AuNPs/$Ab_{Cys\ C}$ (n = 3). (E) Amount of $Ab_{Cys\ C}$ adsorbed per 50 μg of AuNPs/$Ab_{Cys\ C}$ and the corresponding adsorbed ratio (n = 3).

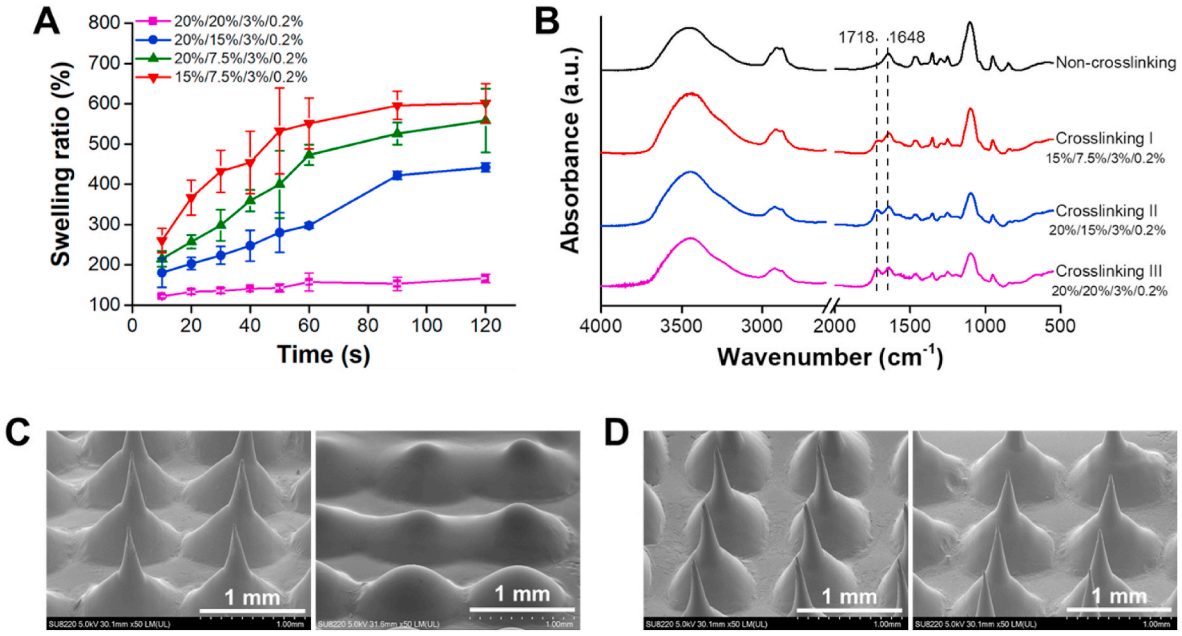

Fig. 2. (A) Swelling ratio (%) of HMNPs prepared with various formulas (PMVE/MA:PEG_{8000}:Na_2CO_3:PAA-Na) at 80 °C crosslinked for 48 h after insertion into a 1% agarose gel (n = 3). (B) FTIR spectra of HMNPs prepared with various formulas (PMVE/MA:PEG_{8000}:Na_2CO_3:PAA-Na) at 80 °C cross-linked for 48 h. (C) Representative SEM images showing the dissolution status of the noncrosslinked MNPs before (left) and after (right) insertion into rat skin for 10 min. (D) Representative SEM images showing the dissolution status of the crosslinked HMNPs before (left) and after (right) insertion into rat skin for 10 min.

showed the highest percentage swelling (601.6 ± 47.9%), followed by HMNPs containing 20% w/w PMVE/MA, 3% w/w Na_2CO_3, and 0.2% w/w PAA-Na crosslinked with 7.5% w/w (558.3 ± 79.3%), 15% w/w (441.9 ± 11.3%), and 20% w/w (116.4 ± 10.7%) PEG_{8000}, respectively. The percentage swelling may be related to the crosslinking level of PMVE/MA crosslinked with PEG_{8000}. To prove this hypothesis, we investigated the crosslinking level of PEG_{8000}-crosslinked PMVE/MA with different ratios using Fourier transform infrared (FTIR) spectroscopy (Fig. 2B). The main difference that can be seen in the spectra of the crosslinked films in contrast with the noncrosslinked films is the presence of a new band at 1718 cm^{-1}. This band can be attributed to the new ester carbonyl bonds (C═O) formed between the PMVE/MA acid groups and the alcoholic groups (OH) of PEG_{8000}; a higher intensity means a higher crosslinking level. The results demonstrated that 20% w/w PMVE/MA crosslinked with 20% w/w PEG_{8000} showed the highest crosslinking level, followed by 20% w/w PMVE/MA crosslinked with 15% w/w PEG_{8000} and 15% w/w PMVE/MA crosslinked with 7.5% w/w PEG_{8000}. The above results indicated that HMNPs made of 15% w/w PMVE/MA, 7.5% w/w, 3% w/w Na_2CO_3 and 0.2% w/w PAA-Na showed the best swelling property and a failure force of 0.34 N per needle

(Fig. S3), which is much larger than the force reportedly required to puncture human skin (approximately 0.058 N per needle) (Liao et al., 2017), indicating that the fabricated HMNPs would be strong enough to penetrate skin for skin ISF extraction. The SEM revealed that the resulting HMNPs were 880 μm high and 800 μm wide at the base, the width of pinpoint was only 10.9 μm that was sharp enough to penetrate stratum corneum. Also, the backing layer of HMNP is flexible enough, resulting in the HMNP can be bent to conform to the skin (Fig. S4). We then imaged the dissolution of HMNPs after insertion into the skin over time by SEM images. The results showed that HMNP without cross-linking penetrated and dissolved into the skin: only bases remained on the patch after 10 min of insertion (Fig. 2C). Conversely, the crosslinked HMNP did not dissolve but retained the complete needle shape after 10 min of insertion (Fig. 2D), indicating that the crosslinked HMNP could penetrate the skin and extract the skin ISF for Cys C detection.

In addition to confirming that HMNP can extract skin ISF, we must also determine whether molecules of different molecular weights in the epidermis can still be drawn into HMNP. Therefore, we pressed HMNP on 1% w/w agarose gels containing rhodamine B (0.5 kDa), mCherry protein (31 kDa) or FITC-BSA (67 kDa) for 5 min, rinsed once using PBS to remove the remnants on the surface of HMNP and observed the fluorescence images by fluorescence stereomicroscopy. We found that HMNP displayed red (rhodamine B and mCherry protein) or green (FITC-BSA) fluorescence after insertion and rinsing, indicating that HMNP can efficiently extract molecules with molecular weights from 0.5 kDa to 67 kDa (Fig. 3). Therefore, extracting Cys C (13 kDa) from skin ISF using HMNP is feasible for the rapid CKD test.

Although we have demonstrated that HMNP has an excellent ISF extraction ability in a 1% agarose gel skin model, the ISF extraction ability of HMNP in rat skin must also be investigated. Therefore, HMNP was pressed into rat skin using thumb force and held under constant pressure for 5 min. After removal of the patch, a pattern of 10 x 10 red fluorescence arrays was clearly observed on the skin surface with staining by rhodamine B (Fig. 4A). Simultaneously, the MNs swelled and slightly deformed, and the colour changed to translucent from white while maintaining their intact structures (Fig. 4B). HMNP was pressed on the back of the rat for a period of 5 min and then weighed after being detached to calculate the amount of extracted ISF at each time point (60, 120, 180, and 300 s). We found that the percentage swelling of HMNP after insertion in rat skin was 195.6 ± 11.3%, which was much lower than that of HMNP after insertion in a 1% agarose gel (601.6 ± 47.9%), most likely because the volume of skin ISF was small. Approximately 24.2 ± 1.7 mg (μL) was extracted from rat skin by HMNP after insertion for 5 min (Fig. 4C), which has been higher than those extracted by PVA/CS hydrogel MNs (approximately 7.5 μL; He et al., 2020) and Osmosis-powered hydrogel MNs (approximately 15 μL; Zheng et al., 2020) in the same duration. Most likely because the formulation with absorbent material (PAA-Na) addition for HMNP preparation can help increase its swelling rate and water absorption.

3.4. $LFC_{Cys\ C}$ performance for Cys C detection

Under optimal experimental conditions, the performance of $LFC_{Cys\ C}$ in Cys C detection was evaluated. As shown in Fig. 5A, as the concentration of Cys C continued to increase, the colour of the T1 line gradually increased, and the T2 line started to appear when the concentration of Cys C was above the threshold. To confirm that the $LFC_{Cys\ C}$ has good selectivity, four proteins often found in ISF were dropped on the $LFC_{Cys\ C}$. The selectivity of $LFC_{Cys\ C}$ was determined by observing the red colour on T1 and T2 lines by the naked eye, while Cys C (5 μg/mL) and PBS were used as the positive and blank controls, respectively. As shown in Fig. 5B, $LFC_{Cys\ C}$ only detects Cys C to display C, T1, and T2 lines, but only the C line appeared in the other groups, indicating that LFC has good selectivity. We further determined the specificity of $LFC_{Cys\ C}$ by stamping Ab_{PSA} (or Ab_{EGFR}) on the detection pad at T1 and T2 zones instead of $Ab_{Cys\ C}$. As shown in Fig. S5, the LFC_{PSA} (Fig. S5b) and LFC_{EGFR} (Fig. S5c) both only displayed C line, no T1 and T2 lines appeared compared to $LFC_{Cys\ C}$ (Fig. S5a), indicating that the stamped Ab_{PSA} (or Ab_{EGFR}) on T1 and T2 lines cannot capture the HRP-*b*-AuNPs/$Ab_{Cys\ C}$-Cys C complexes. The results demonstrated that the $LFC_{Cys\ C}$ not only has good selectivity but also has good specificity.

We then investigated the environmental stability of $LFC_{Cys\ C}$ stored at 37 °C for a period of 28 days, as shown in Fig. 5C. A constant concentration of Cys C (5 μg/mL) was dropped onto $LFC_{Cys\ C}$ stored for each time period to evaluate the stability of the $LFC_{Cys\ C}$ by observing the red colour on the C, T1, and T2 lines. The results showed that all stored $LFC_{Cys\ C}$ displayed C, T1, and T2 lines after storage at 37 °C for a period of 28 days, indicating that the $LFC_{Cys\ C}$ is very stable without loss of recombinant $Ab_{Cys\ C}$ capture activity, even when stored at 37 °C.

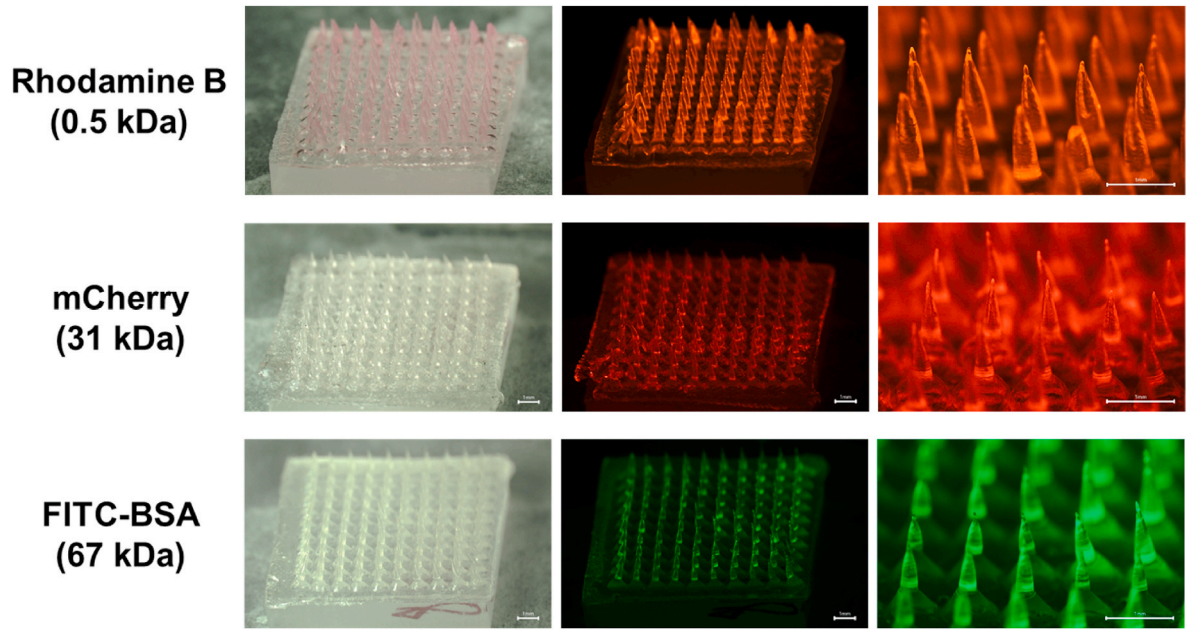

Fig. 3. Images of HMNP after being inserted in a 1% agarose gel containing fluorescent molecules with different molecular weights.

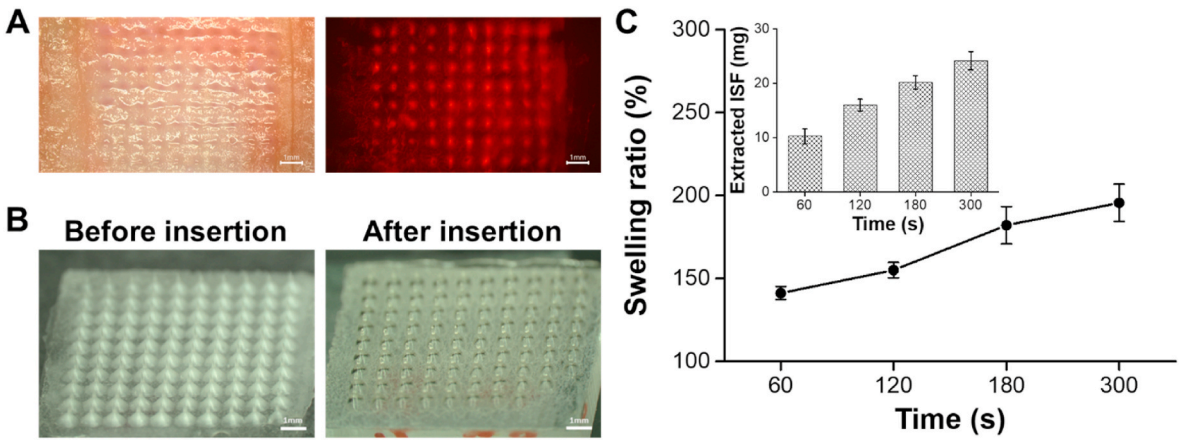

Fig. 4. (A) Bright-field and fluorescence images showing the formation of microcavities and the successful delivery of rhodamine B into rat skin. (B) Bright-field images showing the swelling status of the crosslinked HMNPs before and after insertion into rat skin for 5 min. (C) Swelling ratio (%) of HMNPs after insertion into rat skin for 5 min and the corresponding amount of extracted ISF (n = 3).

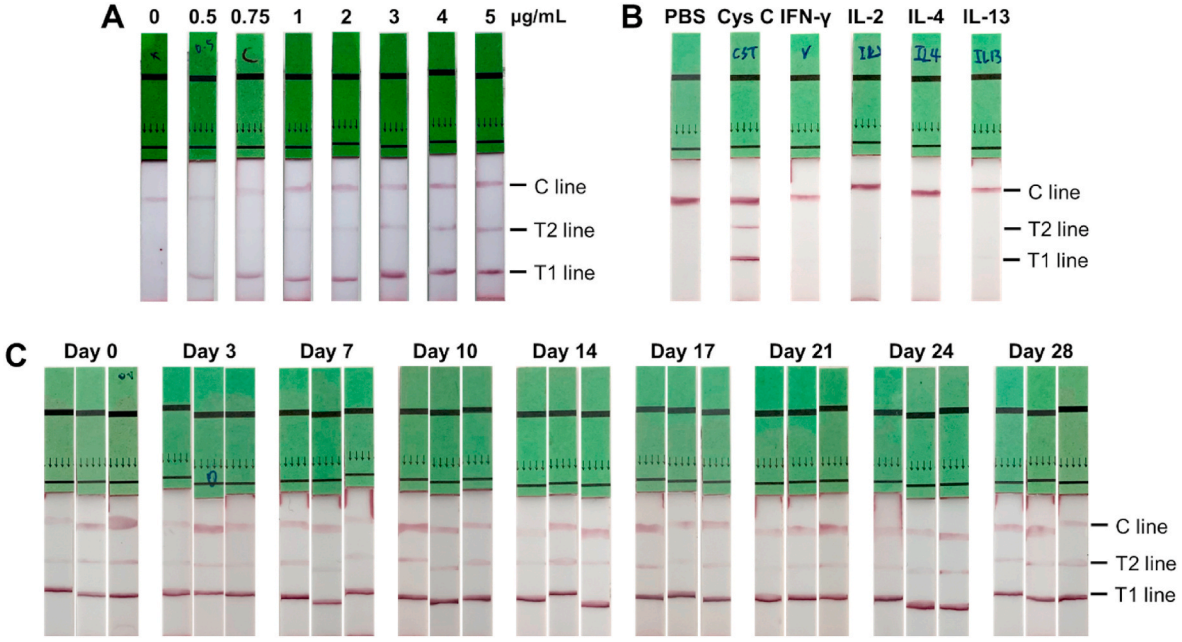

Fig. 5. (A) The sensitivity of $LFC_{Cys\ C}$ for the detection of Cys C. (B) Visual results of the T1 and T2 lines of the $LFC_{Cys\ C}$ in the selectivity assay using various cytokines as interfering substances. (C) Stabilities of the as-prepared $LFC_{Cys\ C}$ stored at 37 °C for a period of 28 days by dropping 5 μg/mL Cys C for testing (n = 3).

3.5. Rapid test of Cys C in ISF of CKD rats

To meet our goal, the HMNPs were thumb pressed into the skin of healthy rats (n = 6) and adenine-induced CKD rats (n = 8) for 5 min to ensure sufficient extraction of the skin ISF before removal. After removal, the needles of HMNP did not dissolve but retained their shape (Fig. 6A), and 100 holes were evident on the skin surface in the shape of the MN array. The procedure was well tolerated by the rats with no significant erythema, oedema or other effects, and within 15 min, the skin almost returned to a normal appearance (Fig. 6B). Finally, the feasibility and performance of instrument-free *in vivo* skin ISF Cys C biosensing using the integration of HMNP and $LFC_{Cys\ C}$ were studied in adenine-induced CKD rats. We first analysed the concentrations of Cys C in serum and skin ISF samples from healthy and CKD rats using ELISA. The concentrations of Cys C in serum collected from healthy and CKD rats were measured as 40.2 ± 6.1 ng/mL and 377.6 ± 42.7 ng/mL, respectively (Fig. 6C). The concentrations of Cys C in skin ISF from healthy and CKD rats were approximately 0.31 ± 0.04 μg/mL and 1.94 ± 0.21 μg/mL, respectively (Fig. 6D). The results confirmed that the concentration of Cys C in skin ISF was much higher than that in serum, and we set the detection threshold for CKD at 1 μg/mL in this study. Based on our design, T1 and T2 lines will appear simultaneously when the concentration of Cys C is higher than the threshold (1 μg/mL), meaning that the subject may suffer from CKD with high risk. To confirm this hypothesis, we have to investigate what concentration of $Ab_{Cys\ C}$ should be stamped on T1 line to effectively capture all HRP-*b*-AuNPs/$Ab_{Cys\ C}$-Cys C complexes, when the detection concentration of Cys C is below the threshold (1 μg/mL). As shown in Fig. S6, the C, T1, and T2 lines were simultaneously appeared on $LFC_{Cys\ C}$ after running the test with 1 μg/mL Cys C, when the $Ab_{Cys\ C}$ stamped on T1 line was 0.5 mg/mL (Fig. S6a). However, when the $Ab_{Cys\ C}$ stamped on T1 line increased to 1 mg/mL (Fig. S6b) and 1.5 mg/mL (Fig. S6c), only C and T1 lines appeared on the $LFC_{Cys\ C}$, indicating that the concentration of $Ab_{Cys\ C}$ stamped on T1 line should be at least 1 mg/mL if the threshold was set as 1 μg/mL for CKD monitoring. Next, we extracted skin ISF from healthy

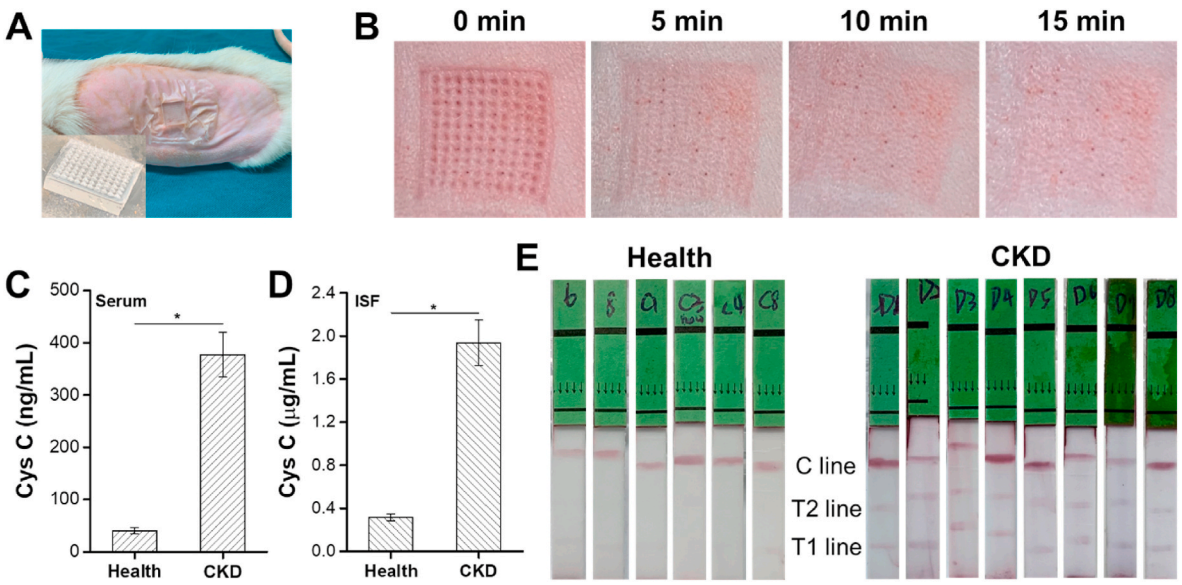

Fig. 6. (A) Representative photographs of rats after insertion of HMNP and detached HMNP after 5 min of insertion (inset). (B) Rat skin puncture marks at a period of 15 min after HMNP removal. (C) The concentration of Cys C in serum collected from healthy (n = 6) and CKD (n = 8) rats by ELISA. *indicates a significant difference (Student's *t*-test, $*p \leq 0.05$). (D) The concentration of Cys C in skin ISF calculated from the ELISA results. *indicates a significant difference (Student's *t*-test, $*p \leq 0.05$). (E) Detection of Cys C by an integration of HMNP and $LFC_{Cys\ C}$ in rat skin ISF samples. The visual results of Cys C in the ISF of healthy rats (n = 6) and CKD rats (n = 8) were analysed by $LFC_{Cys\ C}$ (healthy rats: no red line or only one slight red line observed at T1 zone; CKD rats: two red lines were observed at T1 and T2 zones, respectively).

rats and CKD rats using HMNPs and then directly transferred the HMNPs to $LFC_{Cys\ C}$ for Cys C detection. As shown in Fig. 6E, no red line or only one slight red line was observed at the T1 zone in the group of healthy rats. Conversely, two red lines were observed at the T1 and T2 zones in the group of CKD rats, indicating that the concentration of Cys C in CKD rats was significantly higher than that in healthy rats and the concentrations in skin ISF for the rats with CKD were all higher than 1 μg/mL. No significant difference was found compared with those obtained using ELISA. The results confirm that the concept of using an integration of HMNP and LFC for blood-free CKD monitoring is feasible.

However, the concentrations of Cys C differed in rats and humans. According to previous reports, the physiological concentration of Cys C in the serum of healthy people is approximately 0.72 ± 0.22 μg/mL, the concentrations of Cys C further increased to 0.90 ± 0.15 μg/mL and 1.06 ± 0.23 μg/mL at CKD stage I and II, respectively (Donadio et al., 2012). Moreover, the ISF/serum ratio of Cys C is about 3.5–5.7, with an average of 4.6 (Filler et al., 2005; Tran et al., 2018), resulting in the concentration of Cys C in skin ISF of healthy people is expected to be approximately 3.31 μg/mL then the concentrations of Cys C increased to 4.14 μg/mL 4.89 μg/mL at CKD stage I and stage II, respectively. Thus, the detection threshold for CKD should be adjusted to 4 μg/mL instead of 1 μg/mL for future human studies. We therefore increased the amount of $Ab_{Cys\ C}$ stamped on the T1 line to 2 mg/mL. The results demonstrated that both T1 and T2 lines appeared simultaneously only when the concentration of Cys C was higher than 4 μg/mL (Fig. S7), and the detection threshold setting of $LFC_{Cys\ C}$ can be easily adjusted by changing the amount of $Ab_{Cys\ C}$ stamped on T1 line. Therefore, the developed Cys C rapid test combined with HMNP and $LFC_{Cys\ C}$ has a strong potential POC for distinguishing CKD patients and/or healthy people, ensuring optimal patient management, including available and precise treatment in the time of a pandemic (i.e., COVID-19).

4. Conclusion

In this study, we developed an integration of HMNP and $LFC_{Cys\ C}$, which can be used to rapidly detect Cys C in skin ISF within 25 min (including a 5-min ISF extraction step and a 15-min $LFC_{Cys\ C}$ test step) for blood-free CKD management by the naked eye and no cross-reaction with other cytokines in ISF. HMNP could extract approximately 27.6 ± 1.7 μL of ISF from rat back skin *in vivo*. The large ISF volume collected from the one-time application of this super swelling HMNP could be sufficient for transference of the extracted ISF to the $LFC_{Cys\ C}$ sample pad for biomarker detection. Ultimately, this integration of HMNP and $LFC_{Cys\ C}$ will improve the patient experience in the skin ISF extraction process and greatly benefit personal CKD management during a pandemic.

CRediT authorship contribution statement

Yi-Jyun Chen: Methodology, Software, Validation, Formal analysis, Investigation, Writing – original draft. **Ying-Pei Hsu:** Methodology, Investigation, Software, Formal analysis, Resources. **You-Lin Tain:** Methodology, Investigation, Resources, Animal studies. **Nan-Si Li:** Investigation. **Hao-Han Pang:** Project administration, Resources. **Shiao-Wei Kuo:** Conceptualization, Project administration, Resources, Funding acquisition. **Hung-Wei Yang:** Conceptualization, Methodology, Project administration, Writing – review & editing, Supervision, Funding acquisition.

Declaration of competing interest

The authors declare that they have no known competing financial interests or personal relationships that could have appeared to influence the work reported in this paper.

Acknowledgements

This work was financially supported by the Ministry of Science and Technology, Chang Gung Memorial Hospital, and National Sun Yat-sen University, Taiwan (R.O.C.), for the financial assistance provided (MOST109-2221-E-110-006-MY3, MOST110-2628-B-110-004-, CMRP G8K1011, and 110-02). We would also like to thank the Chang Gung Memorial Hospital Microscopy Core Laboratory for their assistance with the TEM and SEM techniques.

Appendix A. Supplementary data

Supplementary data to this article can be found online at https://doi.org/10.1016/j.bios.2022.114234.

References

Biljak, V.R., Honović, L., Matica, J., Krešić, B., Vojak, S.S., 2017. Biochem. Med. 27, 153–176.

Bodenlenz, M., Tiffner, K.I., Raml, R., Augustin, T., Dragatin, C., Birngruber, T., Schimek, D., Schwagerle, G., Pieber, T.R., Raney, S.G., Kanfer, I., Sinner, F., 2016. Clin. Pharmacokinet. 56, 91–98.

Chang, Y.C., Chu, Y.H., Wang, C.C., Wang, C.H., Tain, Y.L., Yang, H.W., 2021. Biosensors 11, 339.

Desai, D., Kumar, A., Bose, D., Datta, M., 2018. Biosens. Bioelectron. 105, 90–94.

Devi, K.S.S., Krishnan, U.M., 2020. Microchim. Acta 187, 585.

Donnelly, R.F., McCrudden, M.T.C., Alkilani, A.Z., Larrañeta, E., McAlister, E., Courtenay, A.J., Kearney, M.C., Singh, T.R.R., McCarthy, H.O., Kett, V.L., Caffarel-Salvador, E., Al-Zahrani, S., Woolfson, A.D., 2014. PLoS One 9, e111547.

Donadio, C., Kanaki, A., Caprio, F., Donadio, E., Tognotti, D., Olivieri, L., 2012. Nephrol. Dial. Transplant. 27, 2826–2838.

Filler, G., Bökenkamp, A., Hofmann, W., Bricon, T.L., Martínez-Brú, C., Grubb, A., 2005. Clin. Biochem. 38, 1–8.

Gansevoort, R.T., Hilbrands, L.B., 2020. Nat. Rev. Nephrol. 16, 705–706.

Grubb, A., Nyman, U., Björk, J., Lindström, V., Rippe, B., Sterner, G., Christensson, A., 2005. Clin. Chem. 51, 1420–1431.

He, R., Niu, Y., Li, Z., Li, A., Yang, H., Xu, F., Li, F., 2020. Adv. Healthc. Mater. 9, 1901201.

Hsu, W.L., Huang, C.Y., Hsu, Y.P., Hwang, T.L., Chang, S.H., Wang, H.Y.J., Feng, L.Y., Tzou, S.J., Wei, K.C., Yang, H.W., 2020b. Chem. Eng. J. 398, 125536.

Hsu, Y.P., Yang, H.W., Li, N.S., Chen, Y.T., Pang, H.H., Pang, S.T., 2020a. ACS Sens. 5, 928–935.

Kim, S., Lee, M.S., Yang, H.S., Jung, J.H., 2021. Sci. Rep. 11, 14018.

Lesnak, M., Jursa, D., Miskay, M., Riedlova, H., Barcova, K., Adamek, M., 2021. Biotechniques 70, 263–270.

Liao, J.F., Lee, J.C., Lin, C.K., Wei, K.C., Chen, P.Y., Yang, H.W., 2017. Theranostics 7, 2593–2605.

Lopes, P., Costa-Rama, E., Beirão, I., Nouws, H.P.A., Santos-Silva, A., Delerue-Matos, C., 2019. Talanta 201, 211–216.

Madden, J., O'Mahony, C., Thompson, M., O'Riordan, A., Galvin, P., 2020. Sens. Biosens. Res. 29, 100348.

Neild, G.H., 2017. Pediatr. Nephrol. 32, 243–248.

Nilsson, A.K., Sjöbom, U., Christenson, K., Hellström, A., 2019. Lipids Health Dis. 18, 164.

Pacielloab, A., Santonicola, M.G., 2015. RSC Adv. 5, 88866–88875.

Samant, P.P., Niedzwiecki, M.M., Raviele, N., Tran, V., MenaLapaix, J., Walker, D.I., Felner, E.I., Jones, D.P., Miller, G.W., Prausnitz, M.R., 2020. Sci. Transl. Med. 12, eaaw0285.

Sarnak, M.J., Levey, A.S., Schoolwerth, A.C., Coresh, J., Culleton, B., Hamm, L.L., McCullough, P.A., Kasiske, B.L., Kelepouris, E., Klag, M.J., Parfrey, P., Pfeffer, M., Raij, L., Spinosa, D.J., Wilson, P.W., 2003. Circulation 108, 2154–2169.

Sharma, A.P., Yasin, A., Garg, A.X., Filler, G., 2011. Clin. J. Am. Soc. Nephrol. 6, 1599–1608.

Tran, B.Q., Miller, P.R., Taylor, R.M., Boyd, G., Mach, P.M., Rosenzweig, C.N., Baca, J.T., Polsky, R., Glaros, T., 2018. J. Proteome Res. 17, 479–485.

Uchida, K., Gotoh, A., 2002. Clin. Chim. Acta 323, 121–128.

Vart, P., Powe, N.R., McCulloch, C.E., Saran, R., Gillespie, B.W., Saydah, S., Crews, D.C., 2020. JAMA Netw. Open 3, e207932.

Wang, B., Yu, X.A., Yin, G., Wang, J., Jin, Y., Wang, T., 2021. J. Pharm. Biomed. 203, 114230.

Xu, J., Fang, Y., Chen, J., 2021. Biosensors 11, 245.

Zheng, M., Wang, Z., Chang, H., Wang, L., Chew, S.W.T., Lio, D.C.S., Cui, M., Liu, L., Tee, B.C.K., Xu, C., 2020. Adv. Healthc. Mater. 9, 1901683.